analytical chemistry

Article

pubs.acs.org/ac

Terms of Use CC-BY

Bayesian Inference of Accurate Population Sizes and FRET Efficiencies from Single Diffusing Biomolecules

Rebecca R. Murphy,[†] George Danezis,[‡] Mathew H. Horrocks,[†] Sophie E. Jackson,[†] and David Klenerman*,[†]

[†]Department of Chemistry, University of Cambridge, Cambridge CB2 1EW, United Kingdom

[‡]Department of Computer Science, University College London, London WC1E 6BT, United Kingdom

Supporting Information

ABSTRACT: It is of significant biophysical interest to obtain accurate intramolecular distance information and population sizes from single-molecule Förster resonance energy transfer (smFRET) data obtained from biomolecules in solution. Experimental methods of increasing cost and complexity are being developed to improve the accuracy and precision of data collection. However, the analysis of smFRET data sets currently relies on simplistic, and often arbitrary methods, for the selection and denoising of fluorescent bursts. Although these methods are satisfactory for the analysis of simple, low-noise systems with intermediate FRET efficiencies, they display systematic inaccuracies when applied to more complex systems. We have developed an inference method for the analysis of smFRET data from solution studies based on rigorous model-based Bayesian techniques. We implement a Monte Carlo Markov chain (MCMC) based algorithm that simultaneously estimates population sizes and intramolecular distance information directly from a raw smFRET data set, with no intermediate event selection and denoising steps. Here, we present both our parametric model of the smFRET process and the algorithm developed for data analysis. We test the algorithm using a combination of simulated data sets and data from dual-labeled DNA molecules. We demonstrate that our model-based method systematically outperforms threshold-based techniques in accurately inferring both population sizes and intramolecular distances.

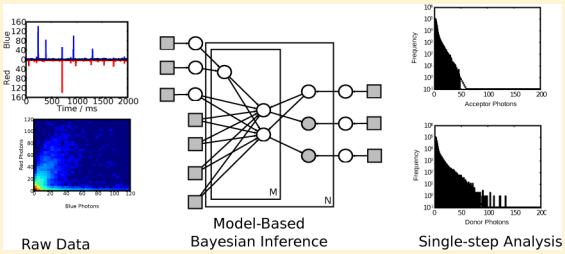

Förster resonance energy transfer (FRET) is a powerful technique for studying biological systems at the level of single molecules. Since the first demonstration that FRET could quantify the distance between two fluorescent dyes,[1] single-molecule FRET (smFRET) has become a popular tool to investigate the structure and dynamics of individual biomolecules, either immobilized on a surface[2−4] or diffusing in solution.[5−7]

FRET is a nonradiative energy transfer from a donor (D) to an acceptor fluorophore (A), where the efficiency of energy transfer (the FRET efficiency, E) depends on their separation, r

$$E = \frac{1}{1 + \left(\frac{r}{R_0}\right)^6} \tag{1}$$

where R_0 is the distance for which the transfer efficiency is 50%.

In a diffusion based smFRET experiment, photons emitted from the donor and acceptor fluorophores are collected in a continuous stream and time binned on a time scale comparable with the average dwell time of a molecule diffusing through the confocal volume. Time bins containing photons from a fluorescent burst are identified by applying a threshold,[8−10] and selected bursts are denoised.[11] FRET efficiencies are calculated for the denoised bins using

$$E = \frac{n_A}{n_A + \gamma \cdot n_D} \tag{2}$$

for n_A and n_D photons in the acceptor and donor channels, respectively, and γ, an experimentally determined instrument-dependent correction factor. Histograms constructed from the calculated FRET efficiencies are fitted with Gaussian distributions to identify fluorescent populations.[1]

Determining intramolecular distance information and population sizes from smFRET experiments, however, remains challenging,[11] as incomplete sample labeling, photophysical artifacts, unequal photon detection, and the stochastic nature of diffusion through the confocal volume[11] as well as linker dynamics[12] hamper development of quantitative smFRET experiments. Many innovative techniques have been developed to address these challenges and improve data quality. Using smFRET data to constrain molecular dynamics simulations can improve accuracy of structural information.[13,14] Linear flow has been used to reduce heterogeneity in confocal dwell time and diffusion pathway.[15,16] Methods to determine correction factors,[17] development of alternating-laser excitation (ALEX) techniques[18−21] and multiparameter fluorescence detection

Received: April 2, 2014
Accepted: August 8, 2014
Published: August 8, 2014

 © 2014 American Chemical Society dx.doi.org/10.1021/ac501188r | Anal. Chem. 2014, 86, 8603−8612

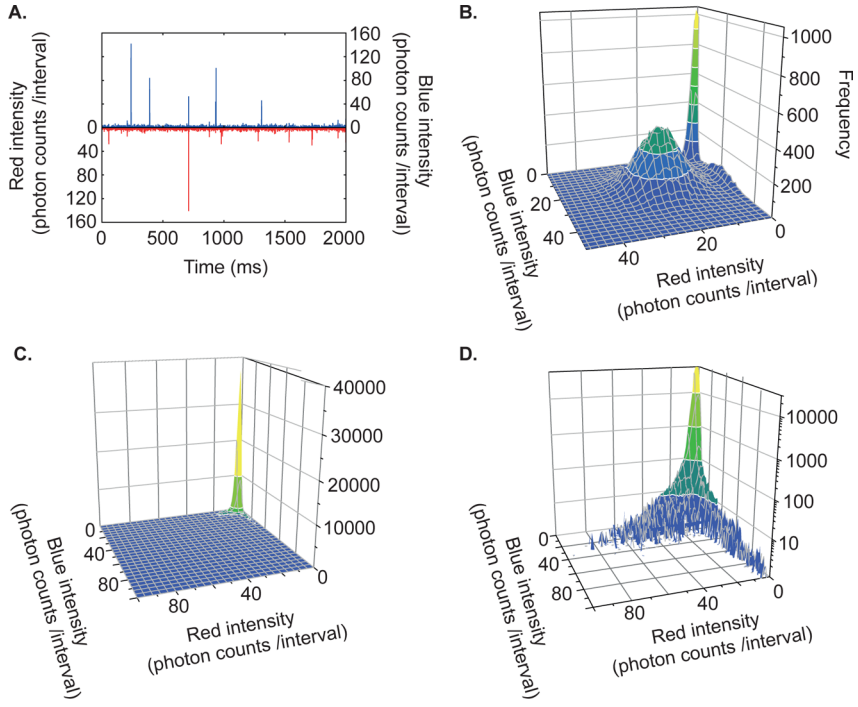

Figure 1. A typical smFRET data set. (A) Snapshot of raw smFRET data from a high-FRET dual-labeled DNA. (B–D) Three-dimensional histograms of raw photon counts from smFRET data sets. (B) An idealized, simulated smFRET data set, with signal and noise well separated, for which thresholding would be a suitable technique for event selection. (C) A real smFRET data set. (D) The same data set shown in panel C plotted on a logarithmic scale to show details of fluorescent bursts.

(MFD)[22] as well as more sophisticated burst-selection algorithms[11,23] allow more accurate identification of fluorescent bursts.

Following burst selection, there is a need to denoise selected bursts. Historically, this has involved subtracting an averaged, nonintegral value from all bursts,[11] often reulting in fractional or negative photon counts, negative FRET efficiencies, and other analysis artifacts. Photon distribution analysis (PDA)[24−27] uses Poisson statistics to stochastically denoise selected bursts. This more sophisticated analysis eliminates unphysical negative photon counts[24] and can accurately predict the width of FRET histograms.[28]

However, these techniques are associated with considerably increased cost and experimental complexity. Furthermore, they assume that fluorescent bursts are clearly distinct from noise and can be separated using an arbitrary cutoff (Figure 1B). However, data from actual smFRET experiments (Figure 1C,D) are not linearly separable, exhibiting significant overlap between the number of noise photons and the number of photons emitted by a fluorescent molecule, meaning that no threshold can perfectly separate photons of interest from noise and making simple fitting of the raw two-dimensional photon distribution (Figure S7) challenging. Consequently, threshold choice is subjective and can significantly influence analytical outcomes[8,9] (Figure S5).

We address these issues by using model-based Bayesian inference to analyze smFRET data. Bayesian inference is a probabilistic method[29] that uses conditional probabilities based on Bayes' theorem[30] to assess the likelihood that a series of observations was generated by a given model.[31] Analysis techniques based on Bayesian statistics are well-established for analysis of smFRET data collected from immobilized molecules.[32−37] Bayesian methods have also been applied to single-particle tracking,[38] analysis of diffusional trajectories,[39,40] fluorescence correlation spectroscopy,[41−44] and fluorescence lifetime data.[45,46] An excellent theoretical understanding of the physical FRET process has been developed by Gopich and Szabo,[47−49] which has facilitated a maximum likelihood approach for the analysis of fluorescent bursts from diffusing molecules.[49,50] However, these methods either do not consider burst selection[49] or apply only to removal of shot noise from selected bursts,[47] so they assume access to idealized simulated,[47] or preselected,[49,50] and denoised fluorescent traces.[45]

Here, we present a simple physical model of the FRET excitation/emission process, incorporating both FRET-based emission and background fluorescence events, which can be used for a single-step analysis of smFRET data from freely diffusing molecules. We use the model as part of a custom-built inference algorithm based on MCMC Metropolis sampling[51] to infer values for all relevant physical parameters, including intramolecular distances and population sizes, conditioned on a smFRET data set. We simultaneously infer all parameters directly from the raw time-binned data, colleted from freely diffusing molecules, in a single step with no intermediate burst selection or denoising. The model is summarized schematically in Figure 2 and described in detail below. The mathematical model describes a Bayesian belief network and is shown as a directed acyclic graph in standard plate notation (Supporting Information Figure S2). We demonstrate this technique's effectiveness using realistic simulated data sets. We then analyze real smFRET data, generated from single populations and mixtures of dual-labeled DNA molecules, showing that our technique can infer physically appropriate and experimentally informative parameters with high confidence across a wide range of conditions. In particular, we accurately infer absolute populations and FRET efficiencies of a mixture of two fluorescent species, where thresholding-based techniques fail.

dx.doi.org/10.1021/ac501188r | Anal. Chem. 2014, 86, 8603−8612

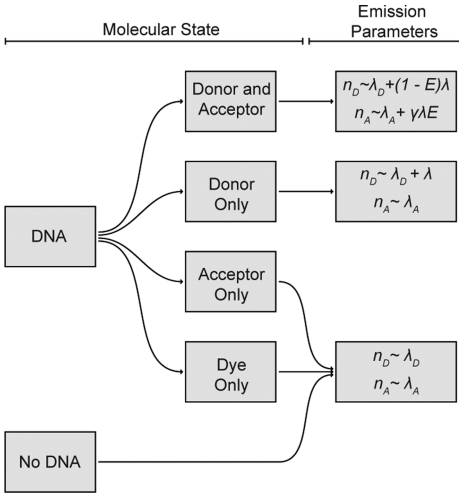

Figure 2. Flow diagram illustrating the generative model for a single FRET population. The molecular state is the underlying state of the current observation; the emission parameters are the Poisson parameters that result in observable photon emission, and they are shown for both donor and acceptor channels.

Here, we discuss only time-binned fluorescence data from continuous excitation experiments. The additional information from alternating excitation methods and the rate of photon arrivals could also be incorporated into a model for inference analysis, but this is not considered here.

THEORY

A Physical Model of a smFRET Experiment. Thus far, analysis of smFRET data has not separated a defined model of the physical process from data analysis. As a consequence, implicit assumptions about the physical model may be reproduced during analysis.[10] Our key innovation is development of a model-based Bayesian analysis. This analysis uses a parametric model of the physical emission process. We then infer values for these parameters given a specific data set to learn information about intramolecular distances and population sizes for different fluorescent species. The model of photon emission in the presence of both dyes is inspired by the traditional model of FRET efficiency (eq 2). However, we model the energy transfer as altering the underlying rates of dye photon emission, whereas traditional techniques use the ratio of donor and acceptor photons observed.

In a basic smFRET experiment, fluorescently labeled molecules in dilute solution diffuse freely through a laser beam focused with a high aperture objective onto a diffraction-limited focal point.[52] When a molecule diffuses into the confocal volume, the laser excites the donor fluorophore, and photons are emitted. Emitted photons are collected through the objective and separated by a dichroic mirror into donor and acceptor photons for collection and analysis (Figure S1A).

These experiments yield bursts of donor and acceptor fluorescence, caused by diffusion of a labeled molecule through the excitation volume, against a background of low-to-zero fluorescence detection. Although accurate arrival times can be recorded,[53] raw data is often collected as two synchronized streams of time-binned photons, corresponding to detected photons with wavelengths in the donor and acceptor emission regions (Figure 1A). The majority of bins (>95%) contain only background noise; the rest contain both background noise and photons from fluorescent bursts (Figure 1C,D).

We model a smFRET data set as a sequence of pairs of measurements (f_D, f_A) of the number of photons observed in the donor and acceptor channels. Each pair of measurements is treated as an independent and identically distributed sample from a set of random variables describing the data set. Each pair of data points (f_D, f_A) in the data stream is the sum of noise photons and possibly some photons from a fluorescent event.

For simplicity, leakage and direct excitation are not currently considered either for the single population case or for multiple populations. However, these can be added to the model without introducing further complexity. Bleaching of the acceptor fluorophore partway through a bin is also not considered.

The number of noise photons is drawn from a Poisson distribution with rate parameter λ_D for the donor channel and rate λ_A for the acceptor channel. The probability of observing n_D noise photons in the donor channel and n_A in the acceptor channel is

$$n_D \sim \text{Poisson}(n_D; \lambda_D) = \frac{\lambda_D^{n_D}}{n_D!} e^{-\lambda_D}$$
$$n_A \sim \text{Poisson}(n_A; \lambda_A) = \frac{\lambda_A^{n_A}}{n_A!} e^{-\lambda_A} \quad (3)$$

In addition to noise, each observation may contain photons from one or more fluorescent molecules. For a data set with a single fluorescent population, the number of molecules present in the excitation volume, n_{DNA}, follows a Poisson distribution with rate parameter λ_{DNA}

$$n_{DNA} \sim \text{Poisson}(n_{DNA}; \lambda_{DNA}) = \frac{\lambda_{DNA}^{n_{DNA}}}{n_{DNA}!} e^{-\lambda_{DNA}} \quad (4)$$

The probability of seeing any molecule is typically low: λ_{DNA} is small and $n_{DNA} = 0$ for the majority of time bins. However, multiple-occupancy events may occur.

We extend this model to describe two or more fluorescent species with different FRET efficiencies and population sizes. Here, the number of molecules of each species is determined independently, with n_{DNA1} and n_{DNA2}, the number of molecules observed of species 1 and 2, respectively, given by

$$n_{DNA1} \sim \text{Poisson}(n_{DNA1}; \lambda_{DNA1}) = \frac{\lambda_{DNA1}^{n_{DNA1}}}{n_{DNA1}!} e^{-\lambda_{DNA1}} \quad (5)$$

and

$$n_{DNA2} \sim \text{Poisson}(n_{DNA2}; \lambda_{DNA2}) = \frac{\lambda_{DNA2}^{n_{DNA2}}}{n_{DNA2}!} e^{-\lambda_{DNA2}} \quad (6)$$

As before, most bins contain no fluorescent molecules ($n_{DNA2} = n_{DNA2} = 0$), but multiple occupancy can be modeled when $n_{DNA2} + n_{DNA2} > 1$.

Each molecule present may be in one of four labeling states: unlabeled, donor only, acceptor only, or dual labeled (Figure S1B). We model the presence of donor and acceptor dyes as independent events with respective probabilities p_D and p_A. Thus, the molecule is unlabeled with probability $(1 - p_D)(1 - p_A)$, both dyes are present with probability $p_D p_A$, and only the acceptor or only the donor dye with probability $p_A(1 - p_D)$ and $(1 - p_A)p_D$, respectively. For multiple fluorescent populations, we assume that all species share the same labeling probabilities, p_D and p_A.

dx.doi.org/10.1021/ac501188r | Anal. Chem. 2014, 86, 8603−8612

Table 1. Parameters Used in the Generation of Synthetic Data

parameter	λ_{DNA}	λ_D	λ_A	p_D	p_A	k_D	λ_B	R_0 (Å)	γ
value	0.06	1.0	1.0	0.6	0.8	1.0	20.0	56.0	1.0

An unlabeled or acceptor-only labeled molecule is not excited, so only background noise is observed; thus, $f_D = n_D$ and $f_A = n_A$.

When a donor dye is present, excitation potentially results in emission. This is modeled in two stages: first, a rate of donor emission, λ, is determined for the specific molecule as a random sample from a gamma distribution with shape parameter k_D and mean λ_B (eq 7). This captures the variation in the number of photons emitted by a molecule as a result of the diffusion path taken through the confocal volume and the effect of donor photobleaching partway through an observation.

The choice of a gamma−Poisson mixture model to describe the fluorescence emission behavior was not arbitrary. It is well-understood that photon emission from molecules passing through the confocal volume displays super-Poissonian behavior,[54] where the population variance exceeds the mean, owing to the inhomogeneous excitation profile. The negative binomial distribution is a very well characterized, and the popular probability distribution for modeling overdispersed data for which all observations are positive.[55,56] It can be parametrized as a gamma−Poisson mixture,[55] where emission behavior follows a Poisson distribution with gamma-distributed intensity. Under this parametrization, λ_B is the global mean emission rate of photons, while the shape parameter k_D describes the degree of overdispersion caused by confocal volume inhomogeneity.

$$\lambda \sim \text{gamma}(\lambda;\, k_D,\, \theta) = \frac{1}{\Gamma(k_D)\theta^{k_D}}\lambda^{(k_D-1)}\, e^{-\lambda/\theta} \quad \text{for } \theta = \lambda_B/k_D \tag{7}$$

where Γ is the gamma function.

Because the confocal volume is fixed and emission from the dye is a fundamental property of the dye−laser interaction, the same k_D and λ_B are used for all fluorescent populations.

If only the donor dye is present, additional photons are observed in the donor channel only. These are drawn from a Poisson distribution with rate parameter λ, where λ is determined uniquely for each molecule using eq 7. The number of additional photons is then c_D

$$c_D \sim \text{Poisson}(c_D;\, \lambda) \tag{8}$$

the total observed photons in the donor channel, f_D, is then the sum $n_D + c_D$; in the acceptor channel, only noise photons, n_A, are observed.

The interesting case is when both dyes are present. In this case, some of the excitation energy is transferred to the acceptor dye, resulting in emission of acceptor photons and attenuation of donor emission. Emission by both donor and acceptor dyes is modeled by drawing photons from Poisson distributions. In a single population data set, the rate of donor photon emission is now $\lambda(1 - E)$, whereas the acceptor rate of photon emission is $\lambda\gamma E$. Here, E is the efficiency of energy transfer (eq 1), λ is the unattenuated rate of donor photon emission associated with the observed molecule, and γ is an instrumental correction factor (eq 2). The additional photons in each channel, c_D and c_A, are thus distributed as

$$c_D \sim \text{Poisson}(c_D;\, \lambda(1 - E)) \text{ and } c_A \sim \text{Poisson}(c_A;\, \gamma\lambda E) \tag{9}$$

The total number of photons in the donor and acceptor channels are thus $f_D = n_D + c_D$ and $f_A = n_A + c_A$, respectively.

For two populations, molecules from different populations exhibit different FRET efficiencies: E_1 for the first population and E_2 for the second. This gives donor and acceptor emission rates, respectively, c_{D1} and c_{A1}, from the first fluorescent population to be

$$c_{D1} \sim \text{Poisson}(c_{D1};\, \lambda(1 - E_1)) \text{ and } c_{A1} \sim \text{Poisson}(c_{A1};\, \gamma\lambda E_1) \tag{10}$$

Similarly, for the second population, c_{D2} and c_{A2} are given by

$$c_{D2} \sim \text{Poisson}(c_{D2};\, \lambda(1 - E_2)) \text{ and } c_{A2} \sim \text{Poisson}(c_{A2};\, \gamma\lambda E_2) \tag{11}$$

The total number of photons is then given by the sum of photons from all fluorescent species currently present and any noise photons: $f_D = c_{D1} + c_{D2} + n_D$ for the donor and $f_A = c_{A1} + c_{A2} + n_A$ for the acceptor channel.

This process is then repeated for each time bin in a data set. This gives two data streams of integer photon counts, corresponding to the donor and acceptor channels in a FRET experiment, representing background noise alone or a combination of noise and excitation events.

This model can be used, with appropriate parameters (Table 1), to generate synthetic data. Comparison of these synthetic photon streams with experimental data reveals an excellent replication of all aspects of the experimental data (see Supporting Information, Figure S4), suggesting that, despite its many simplifications, such as the neglect of direct excitation and leakage effects, this model captures the most important features sufficient to analyze the FRET process.

Inference of Model Parameters. Our key innovation is the use of Bayesian model-based multivariate statistical methods to infer the model parameters of the FRET experiment. Given the generative model of the physical process described in the previous section, we use the calculus of probabilities and Bayes' theorem to derive the joint distribution over all model parameters to be estimated.

Estimating the parameters of a complex model given some experimental observations is a typical inference problem. In a smFRET experiment, we want to determine the concentrations of the fluorescently labeled species and their respective interdye distances given some experimental data. We might also like to know other associated parameters, such as the rate of noise in each channel and the average brightness of fluorescent events. These values are described explicitly as parameters in our generative model. However, due to noise or a small amount of data, as well as the codependence of all observations on all parameters, it is difficult to determine the values of these parameters directly from observations. Consequently, a different strategy must be applied, and probabilistic inference provides a solution. Here, Bayesian inference allows us to co-estimate the values of all parameters of interest. Inference techniques, such as reversible jump Monte Carlo[57] can also

dx.doi.org/10.1021/ac501188r | Anal. Chem. 2014, 86, 8603−8612

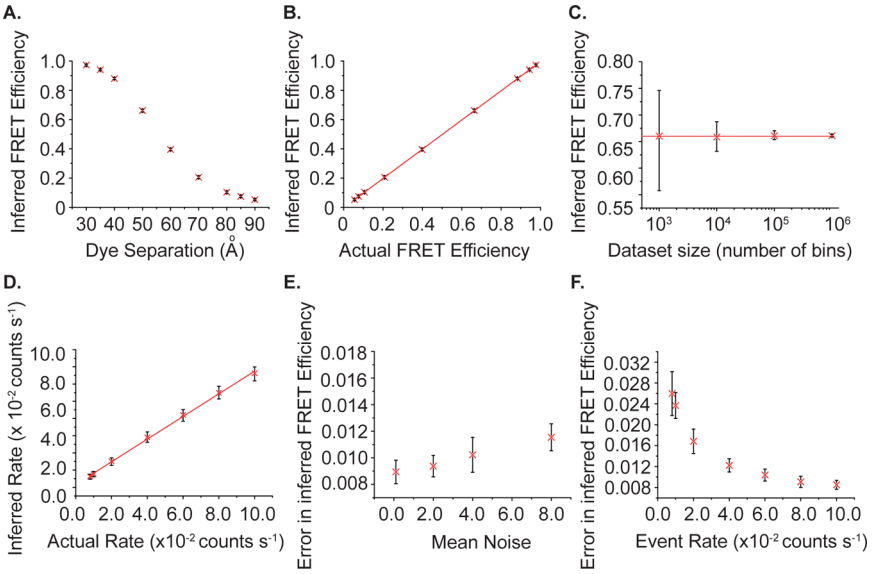

Figure 3. Validation of inference technique using realistic simulated data sets. (A) Inferred FRET efficiency plotted against dye−dye distance. (B) Inferred FRET efficiency plotted against calculated FRET efficiency. (C) Mean inferred FRET efficiency plotted against data set size for synthetic data sets with a dye−dye distance of 60 Å. (D) Inferred population size plotted against actual population size for synthetic data sets with a dye−dye distance of 60 Å. (E) Error in inferred FRET efficiency plotted against the mean value of background noise per time bin. The indicated mean noise was used in both the donor and acceptor channels. The synthetic data sets used a dye−dye distance of 60 Å. (F) Error in inferred FRET efficiency plotted against the rate of observation of labeled molecules for synthetic data sets with a dye−dye distance of 60 Å. All data points on A−F were created using 10 synthetic data sets, generated independently from the same starting parameters. These data sets were analyzed independently using the inference method, generating 98 accepted samples per data set. Shown are the mean values of all accepted samples. The error bars are the values of the highest and the lowest accepted sample values, corresponding to a confidence interval within which the real value lies with probability >99%.

allow for model selection, for example to infer the number of fluorescent populations, but this is not considered here.

Using probability theory, this inference problem is expressed as determining the conditional probability distribution over the parameters given the observations, namely, $\Pr[\lambda_D,\lambda_A,\lambda_D,\lambda_{DNA},\lambda_B,E \mid (f_D f_A)_n]$ for a smFRET data set with n time bins. Given a generative model of the experiment that describes the probability of generating certain observations given known parameters, namely, $\Pr[\mathrm{Obs}|\mathrm{Par}]$, we can apply Bayes' theorem to derive the required distribution over parameters

$$\begin{aligned}&\Pr[\lambda_D, \lambda_A, \lambda_{DNA}, \lambda_B, E|(f_D, f_A)_n]\\ &= \left(\Pr[(f_D, f_A)_n|\lambda_D, \lambda_A, \lambda_{DNA}, \lambda_B, E]\cdot\Pr[\lambda_D, \lambda_A, \lambda_{DNA}, \lambda_B, E]\right)\\ &\quad /\left(\sum_{\forall \lambda_D,\lambda_A,\lambda_{DNA},\lambda_B,E} \Pr[(f_D, f_A)_n|\lambda_D, \lambda_A, \lambda_{DNA}, \lambda_B, E]\cdot\right.\\ &\quad \left.\Pr[\lambda_D, \lambda_A, \lambda_{DNA}, \lambda_B, E]\right)\end{aligned} \tag{12}$$

The term $\Pr[\lambda_D, \lambda_A, \lambda_{DNA}, \lambda_B, E]$ encodes prior information about the parameters, while the denominator, $\sum_{\forall \lambda_D, \lambda_A, \lambda_D, \lambda_{DNA}, \lambda_B, E} \Pr[(f_D, f_A)_n|\lambda_D, \lambda_A, \lambda_{DNA}, \lambda_B, E]\cdot\Pr[\lambda_D, \lambda_A, \lambda_{DNA}, \lambda_B, E]$, is a normalizing factor over all parameter space. Exact evaluation of this expression is often impossible because it is hard to derive an analytical expression for this denominator or even to compute it numerically. Consequently, exact evaluation of eq 12 and exact determination of the posterior distribution, $\Pr[\lambda_D, \lambda_A, \lambda_D, \lambda_{DNA}, \lambda_B, E|(f_D, f_A)_n]$, is not possible.

However, to estimate the distribution of values taken by the parameters of interest, it is not necessary to evaluate eq 12 exactly. It is sufficient to draw parameter samples distributed proportionally to the posterior distribution, $\Pr[(f_D, f_A)_n|\lambda_D, \lambda_A, \lambda_{DNA}, \lambda_B, E]\cdot\Pr[\lambda_D, \lambda_A, \lambda_{DNA}, \lambda_B, E]$.[51] The mean, variance, and quantiles of these samples can be used to estimate the required parameters. Consequently, we can determine the parameter distribution (dye−dye distance, concentration, etc.) most likely to have generated a particular data set by using a Monte Carlo method to sample many possible parameter values and calculating the probability that these parameters generated our data.

The Metropolis algorithm[58,51] is an MCMC algorithm that can be used to sample parameter space for candidate parameter values. It defines the structure of a Markov chain that has as its stationary probability the posterior probability over the model parameters, here $\Pr[(f_D, f_A)_n|\lambda_D, \lambda_A, \lambda_{DNA}, \lambda_B, E]\cdot\Pr[\lambda_D, \lambda_A, \lambda_{DNA}, \lambda_B, E]$. By performing long random walks over that chain, we can generate independent samples of the parameters distributed according to eq 12. Metropolis[59] provides an introduction to the algorithm; our implementation is described in the Supporting Information.

METHODS

Generation of Simulated Data. Simulated data sets were generated using the model described above, using code written in Python. Code is available online (https://bitbucket.org/rebecca_roisin/fret-inference).

smFRET Measurements. Single-molecule data were collected using a custom built system, as described previously.[60] Details of the instrumentation and DNA duplex preparation are found in the Supporting Information. Data were collected for 30 min at room temperature using a 1 ms bin time, in frames of 10 000 bins.

Analysis of Single-Molecule FRET Data. Thresholding-based data analysis was carried out in the standard manner[8] (see Supporting Information). For the inference process, data were fitted in a single step. Raw data, prior to any denoising or

dx.doi.org/10.1021/ac501188r | Anal. Chem. 2014, 86, 8603−8612

event selection steps, were analyzed using the Metropolis sampling process described above. Sampling occurred in two steps. First, two approximate samples were generated, with a burn-in of 3000 iterations and 1000 iterations between samples. Then, 100 further samples were made, with a burn-in of 1000 iterations and 100 iterations between samples. For all analyses, the initial parameters shown in Table 1 were used. The outcome of the inference was not sensitive to initial conditions (see Figure S3). A typical analysis takes approximately 15 min running on a single core. Performance improvements could be achieved by parallelizing the iterative sampling process.

RESULTS

Validation Using Simulated Data. *Single Fluorescent Species.* To validate the inference method, we used the forward model to generate realistic simulated data sets with known parameters. We then analyzed these data sets using the inference method to see how accurately the model parameters could be inferred. We varied several aspects of the simulated data, including mean dye−dye separation (altering E), data set size, mean noise level, and rate of observation of labeled molecules. Unless otherwise stated, parameters used in data generation are those shown in Table 1. The results are summarized in Figure 3. Figure 3A,B shows the FRET efficiencies inferred for data sets with dye−dye distances across the spectrum of FRET efficiencies. From Figure 3A, it can be seen that the inference method correctly reproduces the expected sigmoidal curve of FRET efficiency against dye separation, whereas Figure 3B shows a linear relationship between actual and inferred FRET efficiencies, with tight confidence intervals, demonstrating that the inference method exactly reproduces the values used to generate the simulated data. Similarly, Figure 3D shows that the inference method also correctly infers the rate at which fluorescent events are observed (analogous to concentration), demonstrating a linear relationship between the rate used for data set generation and the rate inferred. The inferred value remains accurate even for very high and very low rates, showing that the method is robust over a wide range of conditions.

Figure 3C shows the variation in the size of the confidence interval with the number of time bins in a data set. Even for a small data set of only 1000 time bins, the inferred mean FRET efficiency was inferred exactly correctly (actual value 0.66, inferred mean 0.66), although the 98% confidence interval (CI98) is very wide (CI98: 056−0.75), as there are insufficient data to allow precise estimation. Making the data set larger significantly reduces the size of the confidence interval, with very narrow intervals for data sets of 100 000 bins or larger (mean: 0.66, CI98: 0.65−0.67). Assuming a bin time of 1 ms, a typical experimental data set (10−20 min of data) would include 6−12 million bins. Consequently, it is a significant achievement of the inference method that it makes extremely accurate estimates of the FRET efficiency using only 100 000 bins, corresponding to less than 2 min of data.

Figure 3E,F shows the effect of noise and observation rate on the size of the confidence interval for the inferred FRET efficiency. As expected, both increased noise and a lower rate (lower concentration of fluorescent molecules) result in a wider confidence interval, reducing how accurately we can infer *E*. However, even when a very low rate or very high noise is used, the size of the error remains small (±0.03 and ±0.01, respectively), meaning that the inference method still gives accurate values.

Finally, it is important to be sure that our simple model can be used to accurately infer known parameters on data sets that we did not simulate using the model itself. We prepared further simulations using the SimFCS software package[61] and analyzed them using inference. The results are shown in Figure S6. As can be clearly seen, the inference model is able to infer exactly the simulated FRET efficiency over a wide range of simulated values (Figure S6A), even under conditions of high noise (Figure S6B) or when simulated data collection times were extremely short (Figure S6C). We were also able to correctly infer the rate at which fluorescent events occurred, although the confidence intervals are wider (Figure S6D).

These results are clear validation that the inference method works reliably across a wide range of data sets. However, a more important question is whether inference can outperform thresholding. To determine this, we analyzed a series of simulated data sets using AND and SUM thresholding and using inference. The results, summarized in Figure 4, show that inference and thresholding are equally good at determining FRET efficiency, but that inference far outperforms thresholding in determining population sizes.

Figure 4A (top panel) shows the FRET efficiencies estimated by inference and by thresholding. All three techniques

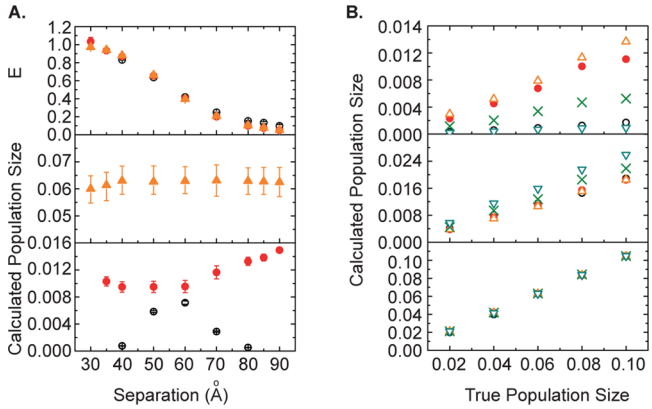

Figure 4. Comparison of the inference technique with thresholding-based methodologies. In all plots (A, B), values shown are from 10 data sets generated independently from the same parameters. For thresholding analyses, error bars represent the standard deviation in the calculated mean from 10 independent data sets. For the inference technique, error bars are the values of the highest and the lowest accepted sample values, corresponding to a confidence interval within which the real value lies with probability >99%. (A, top) FRET efficiencies calculated for a series of simulated data sets using the inference methodologies and the AND and SUM thresholding techniques. Orange triangles are the inferred values, open black circles show AND thresholding, red circles show SUM thresholding. (A, middle, bottom) The effect of FRET efficiency on calculated population size. Data were simulated with an event rate of 0.06 over a wide range of FRET efficiencies. The data were then analyzed, and the population sizes were determined using inference (middle) and thresholding (bottom). Orange triangles (middle) are the inferred values and open black circles and closed red circles (bottom) are values calculated using AND and SUM thresholding, respectively. (B) The effect of FRET efficiency on calculated population size, as calculated using AND (top) and SUM (middle) thresholding and the inference method (bottom). The calculated population size is plotted against the value used in data generation for a wide range of FRET efficiencies. Open black circles, orange triangles (point up), red circles, green crosses, and blue triangles (point down) correspond to FRET efficiencies of 0.88, 0.66, 0.40, 0.21, and 0.11, respectively.

dx.doi.org/10.1021/ac501188r | *Anal. Chem.* 2014, 86, 8603−8612

Table 2. FRET Efficiencies and Population Observation Rates Used in the Generation of Simulated Data Sets with Two Fluorescent Populations

E_1	0.88											
λ_{DNA1}	0.02	0.04	0.06	0.02	0.04	0.06	0.02	0.04	0.06	0.02	0.04	0.06
E_2	0.66			0.40			0.21			0.11		
λ_{DNA2}	0.06	0.04	0.02	0.06	0.04	0.02	0.06	0.04	0.02	0.06	0.04	0.02
E_1	0.66											
λ_{DNA1}	0.02	0.04	0.06	0.02	0.04	0.06	0.02	0.04	0.06			
E_2	0.40			0.21			0.11					
λ_{DNA2}	0.06	0.04	0.02	0.06	0.04	0.02	0.06	0.04	0.02			
E_1	0.40						0.21					
λ_{DNA1}	0.02	0.04	0.06	0.02	0.04	0.06	0.02	0.04	0.06			
E_2	0.21			0.11			0.11					
λ_{DNA2}	0.06	0.04	0.02	0.06	0.04	0.02	0.06	0.04	0.02			

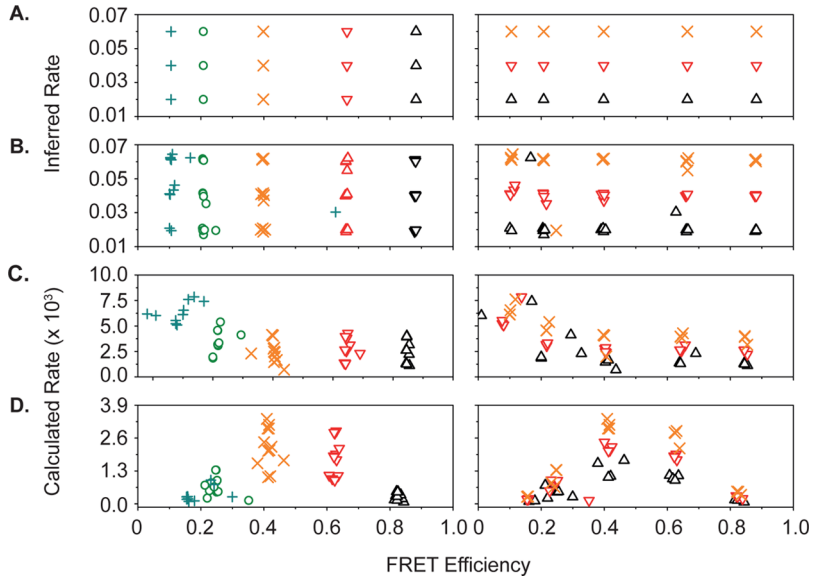

Figure 5. Comparison of inference and thresholding analysis on data sets generated to simulate mixtures of fluorescent species. Calculated population size is plotted against calculated FRET efficiency. (A) Idealized situation in which all FRET efficiencies and population sizes are inferred correctly. (B) Results of analysis using the inference method. (C) Analysis using SUM thresholding. (D) Analysis using AND thresholding. In panels A–D, graphs in the left-hand column are colored according to FRET efficiency: blue crosses (+), green circles, orange crosses (×), red triangles (point down), and black triangles (point up) represent FRET efficiencies of 0.11, 0.21, 0.40, 0.66, and 0.88 respectively. Graphs in the right-hand column are colored according to population size: orange crosses, red triangles (point down), and black triangles (point up) represent, respectively, the large, medium, and small population sizes.

reproduce the characteristic sigmoidal relationship between dye–dye distance and *E*. However, AND thresholding (open black circles) overestimates *E* for the largest distances and was unable to be used for the two smallest separation intervals because too few events were selected to allow histogram construction. These discrepancies are, however, relatively minor, and we see that thresholding performs similarly to inference in determining *E*.

A different story is told, however, when population sizes are considered. Figure 4A (middle and bottom panels) and B compare the ability of thresholding and inference to accurately determine population sizes. The middle and bottom panels of Figure 4A show the relationship between actual and calculated population size for a range of different FRET efficiencies. Here, inference (Figure 4A middle) is clearly superior, showing no variation in the observed population size with FRET efficiency. Both thresholding techniques (Figure 4A bottom) show significant biases in their determined population sizes. First, there is significant underestimation of the overall rate by both AND and SUM thresholding, caused by exclusion of subthreshold events. As the frequency of events decays logarithmically with the number of photons observed (Figure S7), this results in the exculsion of a large number of events. The greatest problems arise from AND thresholding (open circles) where there is significant underestimation of the peak sizes for both high- and low-FRET species. This bias is a direct result of the thresholding analysis: AND thresholding excludes fluorescent events that have a subthreshold number of photons in one channel, but in a high- or low-FRET sample, this excludes most fluorescent events, causing huge underestimation of the population size. A smaller but still significant bias is observed in SUM thresholding (closed circles), which overestimates the populations of low-FRET species relative to higher-FRET species, but it still underestimates the overall rate of fluorescent events. This is caused by inclusion of zero-peak events, which SUM thresholding cannot separate from real events.

A second illustration of this effect is shown in Figure 4B, which shows, for a range of different FRET efficiencies, the relationship between actual and calculated population sizes.

dx.doi.org/10.1021/ac501188r | *Anal. Chem.* 2014, 86, 8603–8612

Both AND (top panel) and SUM (middle panel) thresholding show artifacts in the calculated population sizes. Thresholding results, generally, in an underestimate of the population size, due to exclusion of dim events. Furthermore, AND thresholding (top) considerably underestimates the population sizes for the higest (E = 0.88, open black circles) and lowest (E = 0.11, blue triangles) FRET efficiencies. Similarly, SUM thresholding overestimates the population sizes of the lowest-FRET species (E = 0.11, blue triangles; E = 0.21, green crosses), due to systematic inclusion of zero-peak events. In contrast, inference analysis (bottom) performs well across the full range of dye−dye separations, returning precisely the actual population size for all FRET efficiencies considered. This indicates that inference outperforms thresholding, correctly inferring both E and population size where thresholding cannot.

So far, we have considered simulated data sets containing a single fluorescent population. However, experimental data sets often contain a mixture of several fluorescent species. For a full analysis of these data, all populations must be correctly identified, both in terms of FRET efficiency and population size. To determine the utility of inference in these cases, we generated a total of 30 data sets simulating a mixture of two fluorescent populations using three different population sizes and five different FRET efficiencies. Table 2 summarizes the parameters used. We then analyzed these data sets using inference and using AND and SUM thresholding. The results, shown in Figure 5, demonstrate that inference is significantly superior to both thresholding analyses. Figure 5A shows the expected outcome of analysis of these data, there are five FRET efficiencies and three population sizes, resulting in a grid-like distribution of points. Both AND and SUM thresholding fail to reproduce this outcome. The bias of AND thresholding against high- and low-FRET species creates an inverted U-shaped distribution of calculated event rates (Figure 5D) where species with intermediate FRET efficiencies (0.66 and 0.4) are calculated to have populations many times larger than those with high- or low-FRET efficiencies, even when these species were simulated with a rate three times higher. A different problem is observed in SUM analysis (Figure 5C). Here, although the relative sizes of most populations are inferred correctly, peak areas of low-FRET species are enlarged by confounding with zero-peak events, significantly overestimating these populaton sizes relative to higher-FRET duplexes. Furthermore, SUM thresholding entirely failed to separate mixtures of the two lowest-FRET species (E = 0.21 and 0.11): only a single, broad peak could be fitted. In contrast, inference performs much better, although still imperfectly, at this task. The results of the inference analysis, illustrated in Figure 5B, show good separation of high, medium, and low population sizes and very accurate inference of expected FRET efficiencies. For two data sets, inference does not infer correct values. These data sets both involve the lowest-FRET population (E = 0.11) at its lowest concentration, where it is very difficult to distinguish from noise. In one case, the magnitudes of the two populations (E = 0.11 and 0.21, ratio 1:3) are switched. In the other case (E = 0.11 and 0.66, ratio 1:3), the low-FRET population is ignored, and the high-FRET population is split into two populations with similar values of E. Despite these two failures, it is important to note that whereas inference accurately infers the absolute size of both fluorescent populations in each data set, thresholding techniques not only fail to accurately estimate the absolute population sizes but also frequently estimate incorrectly even the relative sizes of two populations, with inversion of estimated population sizes occurring.

Application to Experimental Data. *DNA Duplexes.* As a first test of the inference technique on experimental data, we determined the FRET efficiencies and population sizes of freely diffusing DNA duplexes labeled with the FRET pair of dyes, Alexa Fluor 488 and Alexa Fluor 647. We also analyzed these data using AND and SUM thresholding. We used a series of different DNA sequences, with dye attachment sites separated by between 4 and 12 bp. As the separation between the dye attachment sites increases, the FRET efficiency is expected to decrease in a sigmoidal manner. As Figure 6 shows, all three

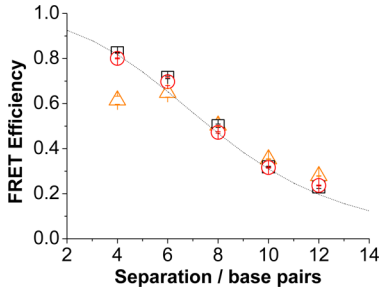

Figure 6. Results of AND, SUM, and inference analysis of smFRET data from single populations of dual-labeled dsDNA. Orange triangles, black squares, and red circles show, respectively, the results of the AND-, SUM-, and inference-based analyses. Error bars show the standard deviation of three independent repeats.

analysis methods reproduce this curve. The discrepancies between these curves are interesting. AND thresholding shows a somewhat squashed curve, with FRET efficiencies of the species with the highest FRET calculated to be lower than calculated by other methods and the species with the lowest FRET efficiencies calculated to have a slightly higher FRET efficiency than by other methods. This is explained by the bias toward intermediate-FRET species that results from the AND criterion. In contrast, both SUM thresholding and the inference process produce a smooth curve without demonstrating this bias.

Mixtures of DNA Duplexes. Finally, we applied two-population inference to mixtures of two DNA duplexes, combined, as in the synthetic examples, in an equimolar ratio (intermediate concentration) or with a 3-fold excess of one duplex (high and low concentrations). We used a high- (4 bp separation), an intermediate- (10 bp separation), and a low-FRET duplex (12 bp separation). The data sets were also analyzed using both AND and SUM thresholding. The results are displayed in Figure 7.

Here, inference (Figure 7A−C) performs very well. In all three cases, the correct FRET efficiency was inferred, and a monotonic increase in event rate is seen among low, intermediate, and high concentrations of duplex. In contrast, the thresholding analyses perform very poorly. FRET efficiencies calculated using AND thresholding (Figure 7D−F) are squashed toward intermediate FRET efficiencies. This also distorts the event distribution, meaning that the population sizes are inaccurately estimated. Similarly, although SUM thresholding (Figure 7G−I) accurately measures FRET efficiencies for two of the mixtures, it is unable to resolve the 10−12 bp mixture, so only a single fluorescent population can be resolved (Figure 7I) . Furthermore, SUM thresholding also

dx.doi.org/10.1021/ac501188r | *Anal. Chem.* 2014, 86, 8603−8612

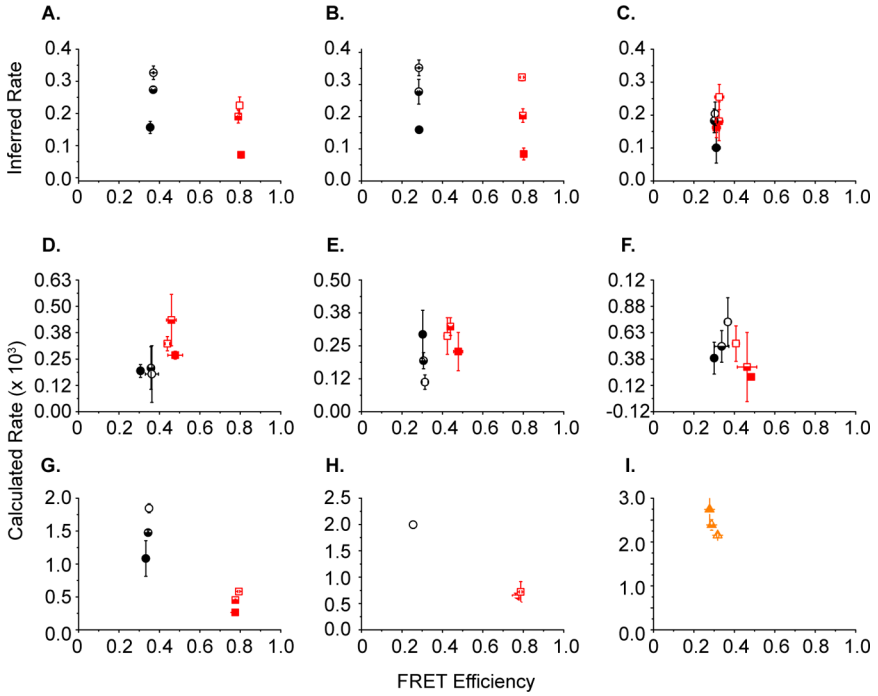

Figure 7. Analysis of a mixture of two populations of dual-labeled dsDNA showing the calculated population sizes and FRET efficiencies. Three different DNA strands were used, with dye attachment sites separated by 4, 10, and 12 bp, corresponding to FRET efficiencies of 0.79, 0.36, and 0.28, respectively, as calculated using the inference method. Two DNA duplexes were combined to give a total DNA concentration of 80 pM, using either 20 pM (low concentration) of one duplex and 60 pM (high concentration) of the other duplex or 40 pM (intermediate concentration) of both duplexes. Black triangles (point up), red triangles (point down), and orange crosses represent the low, intermediate, and high concentrations of DNA, respectively. (A−C) Inference analysis of 4 and 10 bp, 4 and 12 bp, and 10 and 12 bp mixtures, respectively. (D−F) AND analysis of 4 and 10 bp, 4 and 12 bp, and 10 and 12 bp mixtures, respectively. (G−I) SUM analysis of 4 and 10 bp, 4 and 12 bp, and 10 and 12 bp mixtures, respectively. Red squares represent the higher-FRET species in a mixture, and black circles represent the lower-FRET duplex. Open shapes correspond to a concentration of 60 pM (high), whereas filled shapes correspond to a concentration of 20 pM (low). Half-filled shapes correspond to the intermediate duplex concentration of 40 pM. In panel I, SUM analysis was not able to resolve two peaks, so a single Gaussian was fitted. The single peak area and FRET efficiency are shown with orange triangles. Error bars represent the standard deviation of three independent experiments, except in the case of the 3:1 4 bp/10 bp mixture, where one repeat was excluded, due to an incorrect concentration of the 4 bp duplex being used.

distorts the population sizes, with populations of low-FRET species (10 and 12 bp dupelexes) being significantly overestimated, owing to zero-peak contributions. Consequently, inference analysis emerges as the most reliable method to analyze mixtures of fluorescent species. Note, however, that even the inference method cannot fully resolve the 10−12 bp mixture. Although population sizes are correctly inferred, the two FRET efficiencies are compressed toward each other, suggesting that the two species are difficult to distinguish. This indicates a resolution limit of approximately 5 Å for the inference method.

SUMMARY AND CONCLUSIONS

Model-based Bayesian inference is a powerful tool that is used in data analysis across many disciplines.[31] However, despite establishment of model-based inference methods to analyze FRET trajectories from immobilized molecules,[32−36] a similar method had not been developed for smFRET data from molecules in solution. We have developed a model-based inference method, based on the Metropolis algorithm, suitable for the analysis of these data sets. This enables unbiased, single-step determination of FRET efficiencies and population sizes for one or more fluorescent species, as well as other parameters of the data set. Raw data is analyzed in a single step directly, requiring neither biased thresholding nor construction and subjective fitting of FRET histograms. It is extremely robust across a wide variety of conditions. Model-based inference is an exciting new avenue for analysis of smFRET data sets. With simple modifications, similar methods could be developed for analysis of data collected using alternating excitation methods, as well as for other types of smFRET experiments. Reversible jump Monte Carlo[57] provides a promising avenue to infer the number of fluorescent populations, while the additional information available from alternating excitation experiments[18,19] will enable further refinement of the inference analysis. The software for simulation of smFRET data sets and for the analysis of both real and simulated data is available publicly and can be downloaded at https://bitbucket.org/rebecca_roisin/fret-inference.

ASSOCIATED CONTENT

Supporting Information

Methods and derivations as well as a description of the Metropolis algorithm. This material is available free of charge via the Internet at http://pubs.acs.org.

AUTHOR INFORMATION

Corresponding Author

*E-mail: dk10012@cam.ac.uk.

Notes

The authors declare no competing financial interest.

■ ACKNOWLEDGMENTS

R.R.M. thanks BBSRC for research funding. G.D. was employed at Microsoft Research during part of this project.

■ REFERENCES

(1) Ha, T.; Enderle, T.; Ogletree, D. F.; Chemla, D. S.; Selvin, P. R.; Weiss, S. *Proc. Natl. Acad. Sci. U.S.A.* **1996**, *93*, 6264−6268.
(2) Axelrod, D.; Burghardt, T. P.; Thompson, N. L. *Annu. Rev. Biophys. Biomol. Struct.* **1984**, *13*, 247−268.
(3) Axelrod, D. *Traffic* **2001**, *2*, 764−774.
(4) Holden, S. J.; Uphoff, S.; Hohlbein, J.; Yadin, D.; Le Reste, L.; Britton, O. J.; Kapanidis, A. N. *Biophys. J.* **2010**, *99*, 3102−3111.
(5) Haran, G. *J. Phys.: Condens. Matter* **2003**, *15*, R1291−R1317.
(6) Schuler, B.; Lipman, E. A.; Eaton, W. A. *Nature* **2002**, *419*, 743−747.
(7) Weiss, S. *Nat. Struct. Mol. Biol.* **2000**, *7*, 724−729.
(8) Deniz, A. A.; Lawrence, T. A.; Dahan, M.; Chemla, D. S.; Schultz, P. S.; Weiss, S. *Annu. Rev. Phys. Chem.* **2001**, *52*, 233−253.
(9) Gell, C.; Brockwell, D.; Smith, A. *Handbook of Single Molecule Fluorescence*; Oxford University Press: Oxford, 2006.
(10) Ying, L.; Wallace, M. I.; Balsubramanian, S.; Klenerman, D. *J. Phys. Chem. B* **2000**, *104*, 5171−5178.
(11) Nir, E.; Michalet, X.; Hamadani, K. M.; Laurence, T. A.; Neuhauser, D.; Kovchegov, Y.; Weiss, S. *J. Phys. Chem. B* **2006**, *110*, 22103−22124.
(12) Sindbert, S.; Kalinin, S.; Nguyen, H.; Kienzler, A.; Clima, L.; Bannwarth, W.; Appel, B.; Muller, S.; Seidel, C. A. M. *J. Am. Chem. Soc.* **2011**, *133*, 2463−2480.
(13) Kalinin, S.; Peulen, T.; Sindbert, S.; Rothwell, P. J.; Berger, S.; Restle, T.; Goody, R. S.; Gohlke, C. A. M.; Seidel, H. *Nat. Methods* **2012**, *9*, 1218−1225.
(14) Hoefling, M.; Lima, N.; Haenni, D.; Seidel, C. A. M.; Schuler, B.; Grubmüller, H. *PLoS One* **2011**, *6*, e19791.
(15) Vogelsang, J.; Doose, S.; Sauer, M.; Tinnefeld, P. *Anal. Chem.* **2007**, *79*, 7367−7375.
(16) Horrocks, M. H.; Li, H.; Shim, J.; Ranasinghe, R. T.; Clarke, R. W.; Huck, W. T. S.; Abell, C.; Klenerman, D. *Anal. Chem.* **2012**, *84*, 179−185.
(17) Deniz, A.; Laurence, T.; Grunwell, J.; Ha, A.; an Faulhaber, T. J.; Chemla, D.; Weiss, S.; Schultz, P. *Proc. Natl. Acad. Sci. U.S.A.* **1999**, *96*, 3670−3675.
(18) Kapanidis, A.; Laurence, T.; Lee, N.; Margeat, E.; Kong, X.; Weiss, S. *Acc. Chem. Res.* **2005**, *38*, 532−533.
(19) Muller, B. K.; Zaychikov, E.; Brauchle, C.; Lamb, D. C. *Biophys. J.* **2005**, *89*, 3508−3522.
(20) Doose, S.; Heilemann, M.; Michalet, X.; Weiss, S.; Kapanidis, A. N. *Eur. Biophys. J.* **2006**, *36*, 669−674.
(21) Kudryavtsev, V.; Sikor, M.; Kalinin, S.; Mokranjac, D.; Seidel, C. A. M.; Lamb, D. C. *ChemPhysChem* **2012**, *13*, 1060−1078.
(22) Sisamakis, E.; Valeri, A.; Kalinin, S.; Rothwell, P. J.; Seidel, C. A. M. *Methods Enzymol.* **2010**, *475*, 455−514.
(23) Eggeling, C.; Berger, S.; Brand, L.; Fries, J.; Schaffer, J.; Volkmer, A.; Seidel, C. A. M. *J. Biotechnol.* **2001**, *86*, 163−180.
(24) Kalinin, S.; Felekyan, S.; Antonik, M.; Seidel, C. A. M. *J. Phys. Chem. B* **2007**, *111*, 10253−10262.
(25) Antonik, M.; Felekyan, S.; Gaiduk, A.; Seidel, C. A. M. *J. Phys. Chem. B* **2006**, *110*, 6970−6978.
(26) Santoso, Y.; Torella, J. P.; Kapanidis, A. N. *ChemPhysChem* **2010**, *11*, 2209−2219.
(27) Torella, J. P.; Holden, S. J.; Santoso, Y.; Hohlbein, J.; Kapanidis, A. N. *Biophys. J.* **2011**, *107*, 5058−5063.
(28) Kalinin, S.; Valeri, A.; Antonik, M.; Felekyan, S.; Seidel, C. A. M. *J. Phys. Chem. B* **2010**, *114*, 7983−7995.
(29) Barber, D. *Bayesian Reasoning and Machine Learning*; Cambridge University Press: Cambridge, UK, 2012.
(30) Bayes, T.; Price, R. *Philos. Trans. R. Soc. London* **1763**, *53*, 370−418.
(31) MacKay, D. J. *Information Theory, Inference, and Learning Algorithms*; Cambridge University Press: Cambridge, UK, 2003.
(32) McKinney, S. A.; Joo, C.; Ha, T. *Biophys. J.* **2006**, *91*, 1941−1951.
(33) Bronson, J. E.; Fei, J.; Hofman, J. M.; Gonzalez, R. N.; Wiggins, C. H. *Biophys. J.* **2009**, *97*, 3196−3205.
(34) Bronson, J. E.; Hofman, J. M.; Fei, J.; Gonzales, R. L.; Wiggins, C. H. *BMC Bioinf.* **2010**, *11*, 2−10.
(35) Taylor, J. N.; Makarov, D. E.; Landes, C. F. *Biophys. J.* **2010**, *98*, 164−173.
(36) Taylor, J. N.; Landes, C. F. *J. Phys. Chem. B* **2011**, *115*, 1105−1114.
(37) Uphoff, S.; Gryte, K.; Evans, G.; Kapanidis, A. N. *ChemPhysChem* **2011**, *12*, 571−579.
(38) Yoon, J. W.; Bruckbauer, A.; Fitzgerald, W. J.; Klenerman, D. *Biophys. J.* **2008**, *94*, 4932−4947.
(39) Turkcan, S.; Alexandrou, A.; Masson, J.-B. *Biophys. J.* **2012**, *102*, 2288−2298.
(40) Stigler, J.; Rief, M. *ChemPhysChem* **2012**, *13*, 1079−1086.
(41) Kugel, W.; Muschielok, A.; Michaelis, J. *ChemPhysChem* **2011**, *13*, 1013−1022.
(42) Guo, S.-M.; He, J.; Monnier, N.; Sun, G.; Wohland, T.; Bathe, M. *Anal. Chem.* **2011**, *84*, 3880−3888.
(43) He, J.; Guo, S.-M.; Bathe, M. *Anal. Chem.* **2011**, *84*, 3871−3879.
(44) Guo, S.-M.; Bag, N.; Mishra, A.; Wohland, T.; Bathe, M. *Biophys. J.* **2014**, *106*, 190−200.
(45) Kou, S. C.; Xie, X. S.; Liu, J. S. *J. R. Stat. Soc.* **2005**, *54*, 469−496.
(46) Kalinin, S.; Felekyan, S.; Valeri, A.; Seidel, C. A. M. *J. Phys. Chem. B* **2007**, *112*, 8361−8374.
(47) Gopich, I. V.; Szabo, A. *J. Phys. Chem. B* **2007**, *111*, 12925−12932.
(48) Gopich, I. V.; Szabo, A. *J. Phys. Chem. B* **2009**, *113*, 10965−10973.
(49) Gopich, I. V.; Szabo, A. *Proc. Natl. Acad. Sci. U.S.A.* **2012**, *109*, 7747−7752.
(50) DeVore, M. S.; Gull, S. F.; Johnson, C. K. *J. Phys. Chem. B* **2012**, *116*, 4006−4015.
(51) Hastings, W. *Biometrika* **1970**, *57*, 97−109.
(52) Schuler, B. *ChemPhysChem* **2005**, *6*, 1206−1220.
(53) Chung, H. S.; Louis, J. M.; Eaton, W. M. *Proc. Natl. Acad. Sci. U.S.A.* **2009**, *106*, 11837−11844.
(54) Chen, Y.; Muller, J. D.; So, P. T.; Gratton, E. *Biophys. J.* **1999**, *77*, 553−567.
(55) Lloyd-Smith, J. O. *PLoS One* **2007**, *2*, e180.
(56) Bliss, C. I.; Fisher, R. A. *Biometrics* **1953**, *9*, 176−200.
(57) Green, P. J. *Biometrika* **1995**, *82*, 711−732.
(58) Metropolis, N.; Rosenbluth, A. W.; Rosenbluth, M. N.; Teller, A. H.; Teller, E. *J. Chem. Phys.* **1953**, *21*, 1087−1092.
(59) Chib, S.; Greenberg, E. *Am. Stat.* **1995**, *49*, 327−335.
(60) Li, H.; Ying, L.; Green, J. J.; Balasubramanian, S.; Klenerman, D. *Anal. Chem.* **2003**, *75*, 1664−1670.
(61) Gratton, E. *7th International Weber Symposium on Innovative Fluorescence Methodologies in Biochemistry and Medicine*, Kauai, HI, June 6−12, 2008.